American Journal of Electrical and Computer Engineering
2018; 2(2): 5-15
http://www.sciencepublishinggroup.com/j/ajece
doi: 10.11648/j.ajece.20180202.11

Performance Analysis of a 5G Compatible Windowing and Overlapping Scheme Implemented Hybrid Precoded mmWave Massive MIMO NC- OFDM System

Jinia Rahman[1, *], Aniqa Tahsin[2], Shaikh Enayet Ullah[1]

[1]Department of Applied Physics and Electronic Engineering, University of Rajshahi, Rajshahi, Bangladesh

[2]Department of Electrical and Computer Engineering, North South University, Dhaka, Bangladesh

Email address:

jinia4944@gmail.com (J. Rahman), atahsin1828@gmail.com (A. Tahsin), enayet_apee@ru.ac.bd (S. E. Ullah)

[*]Corresponding author

To cite this article:

Jinia Rahman, Aniqa Tahsin, Shaikh Enayet Ullah. Performance Analysis of a 5G Compatible Windowing and Overlapping Scheme Implemented Hybrid Precoded mmWave Massive MIMO NC- OFDM System. *American Journal of Electrical and Computer Engineering*. Vol. 2, No. 2, 2018, pp. 5-15. doi: 10.11648/j.ajece.20180202.11

Received: October 16, 2018; **Accepted**: October 31, 2018; **Published**: November 21, 2018

Abstract: Non-continuous orthogonal frequency division multiplexing (NC-OFDM) can be considered as a promising technique for obtaining significant sidelobe suppression in baseband OFDM signaling. In this paper, we have conducted an investigative study on the performance analysis of a 5G compatible Windowing and overlapping (WO) scheme implemented mmWave massive MIMO NC-OFDM wireless communication system. In such 32×256 massive MIMO antenna configured Hybrid Precoded and 3D beamforming scheme implemented simulated system, various signal detection (Group detection (GD) approach aided and Cholesky decomposition (CD) based efficient Zero-Forcing (ZF)), modern channel coding (LDPC, and (3, 2) SPC)) and windowing and overlapping for Out-of-band(OOB) power spectral reduction techniques have been implemented with higher order digital modulations (64-QAM, 128- QAM and 256-QAM). On consideration of color image transmission in constructed 3D geometrical mmWave Massive MIMO fading channel, it is observable from MATLAB based simulation study that the (3, 2) SPC) channel encoded simulated system is quite robust and effective in retrieving color image under utilization of Cholesky decomposition (CD) based efficient Zero-Forcing (ZF) signal detection techniques. The impact of tapering of Tukey (tapered cosine) window and various order of digital modulations on system performance in terms of Bit error rate(BER) have also been assessed critically. Additionally, it is noticeable that implementation of 2D image noise filtering technique enhances the quality of retrieved color image.

Keywords: NC-OFDM, Windowing and Overlapping, GD and CD Based Zero-Forcing, Modern Channel Coding, Hybrid Precoding, mmWave Geometrical Channel, SNR

1. Introduction

Non-contiguous orthogonal frequency-division multiplexing (NC-OFDM) has been recognized as one of the most suitable candidates for future Fifth Generation (5G) communication with cognitive capabilities. To fulfill the rapidly increasing demands for spectrum resources, academic and industrial communities have given special emphasis on various multicarrier transmission techniques using noncontiguous subcarriers such as Non-contiguous orthogonal frequency-division multiplexing (NC-OFDM), its enhanced version, Generalized multicarrier (GMC) multiplexing, or its special case, namely the Non-contiguous filter-bank multi-carrier (NC-FBMC) technique. The NC-OFDM is often employed as a physical layer technology for Cognitive radio (CR) networks due to its ability to exploit spectrum holes in underutilized licensed bands by adapting to the parameters of wireless communication systems intelligently according to the communication environment [1, 2]. In 2017, Fathima etal. discussed side-lobe suppression methods implemented in a Non-contiguous orthogonal frequency division multiplexing (NC-OFDM) based Cognitive radio (CR) system with utilization of the fixed length rectangular windowing functions for Cancellation carriers (CC's) like Extended active interference cancellation

(EAIC) and Active interference cancellation (AIC) methods [2]. The authors proposed a novel variable basis function in which the CCs were grouped by frequency positions and modeled with different waveforms of different length to suppress the NC-OFDM side lobes effectively while reducing Intercarrier interference (ICI) at the same time. In 2017, Elahi etal., proposed twoalgorithms for the enhancement of spectrum sharing capability such as Genetic algorithm (GA) and Firefly algorithm (FFA)for cancelling OOB radiation by inserting Cancellation carriers (CCs) on either side of the used NC-OFDM signal under consideration of NC-OFDM as an appropriate candidate for Cognitive radio (CR) physical layer [3]. In addressing 5G network architectural designing, three predominant key approaches such as Ultra-dense networks (UDNs), large quantities of new bandwidth and high spectrum efficiency have been taken into consideration. In existing 4G wireless cellular networks, network densification has already been adopted using small cell technology and denser networking would hopefully boost up further network capacity [4]. In 2018, Qin et al., proposed a novel FFT pruning algorithm which reduced computation complexity and improved data rates in 5G in comparison with task of making unnecessary calculation in traditional IFFT/FFT module of NC-OFDM [5]. In 2018, Dan et al., analyzed interference caused by NC-OFDM in terms of power distribution in the frequency domain and proposed an improved NC-OFDM pre-coder aided by optimized subcarrier power allocation to suppress the interference to NC-OFDM systems [6]

In this paper, we have presented simulation results for a non-contiguous orthogonal frequency-division multiplexing wireless communication system under consideration of a large MIMO antenna configuration and implementation of hybrid precoding, Windowing and overlapping (WO) techniques in signal transmission with mmWave carrier frequency.

2. Review of Different Signal Processing Techniques

In this subsection, various signal processing techniques have been implemented. A brief overview of each technique is outlined below:

2.1. Non-Contiguous Orthogonal Frequency-Division Multiplexing

In a non-contiguous orthogonal frequency-division multiplexing (NC-OFDM) scheme, a 1024-sized IFFT block has been considered where the total number of subcarriers is 1024. Out of the 1024 subcarriers, merely 568 subcarriers are treated as active subcarriers for utilizing 568 complex digitally modulated data symbols. The remaining subcarriers are null subcarriers viz. they do not carry any data symbols. All the subcarrier indices are in the range: {-512, -511, - 510…….0, 1, 2, 3,...511} and the active subcarriers indices, IDC= {-400..-245} ∪ {-164,…..-41} ∪ {40,…..163} ∪ {244,…..407}. In this NC-OFDM scheme, no cancellation carriers have been inserted. The 568 data symbols and the remaining 456 zeros are fed into the IFFT block for multicarrier modulation. The active subcarrier indexing is designed based on the idea presented in [1] where all the subcarrier indices are in the range: {-128,-127,-126….0, 1, 2, 3,.. 127} and the active subcarriers indices, IDC ={−100,…,−62} ∪ { −41,…,−11} ∪ {10,…, 40} ∪ {61,…, 101} for a total number of subcarriers 256 and the number of active subcarriers is 142.

2.2. Windowing and Overlapping on the Cyclic Prefix and Postfix

In 5G and B5G future generation wireless networks, spectrum efficiency has become an important component in perspective of Out of band (OOB) spectral power reduction. An etal. proposed a spectrum efficient WO-OFDM technique using windowing and overlapping on the cyclic prefix and postfix [7]. In this technique, CP (Cyclic prefix) addition is performed as conventional multicarrier modulation (OFDM) and some remaining part of the OFDM symbol is copied and added into the right end of the multicarrier modulation symbol. After completion of both the pre and post cyclic fixing, Tukey (Tapered Cosine) windowing technique is applied on the left part of the conventional CP and the right part of the new cyclic postfix. Tukey (Tapered Cosine) windowing technique is quite effective for PAPR reduction [8].

2.3. 3D Geometrical Massive MIMO mmWave Fading Channel Estimation

The narrow-band mmWave Massive MIMO clustered channel with Nt(Nr) number of transmitting (receiving) antenna elements of unity gain can be written as

$$H = \sqrt{\frac{N_t N_r}{N_{c1} N_{ray} \rho_0}} \sum_{i=1}^{N_{c1}} \sum_{l=1}^{N_{ray}} \alpha_{il} a_r(\phi^r_{il}, \theta^r_{il}) a_t(\phi^t_{il}, \theta^t_{il})^H \quad (1)$$

where, N_{cl}(=8) and N_{ray}(=10) represent the number of clusters and the number of rays in each cluster. Here, α_{il} denotes the gain of the lth ray in the ith propagation cluster, $a_r(\phi^r_{il}, \theta^r_{il})$ and $a_t(\phi^t_{il}, \theta^t_{il})$ represent the receive and transmit array response vectors, $\phi^r_{il}(\phi^t_{il}), \theta^r_{il}(\theta^t_{il})$ stand for azimuth and elevation angles of arrival and departure respectively and $\rho_0$is the average path loss. The average path loss is considered using Alpha-beta-gamma (ABG) free space reference distance path loss model presented in [9]. The azimuth and elevation angles of arrival and departure are uniformly Laplacian distribution in [0, 2 π]. The mean values of azimuth and elevation angles of departure are uniformly distributed within the range: - π/2 to + π/2 and standard deviation is of 5 degree. The mean values of azimuth and elevation angles of arrival are uniformly distributed within the range of [0 to 2 π] and [- π/2 to + π/2] respectively with a standard deviation of 5 degree. At the transmitter side, there is a rectangular planner antenna array with nrow1 (=32) × ncol1 (=8) elements. The normalized transmit array response vector corresponding to the lth ray in the ith cluster is givenby:

$$a_t(\phi_{il},\theta_{il})=\frac{1}{\sqrt{nrow1*ncol1}}[1,\ldots,e^{j\frac{2\pi}{\lambda}d(lsin\varphi_{il}sin\theta_{il}+mcos\theta_{il})},\ldots e^{j\frac{2\pi}{\lambda}d\left((nrow-1)sin\varphi_{il}sin\theta_{il}+(ncol-1)cos\theta_{il}\right)}]^T \quad (2)$$

where, l=0, 1, 2……. nrow1, m= 0, 1, 2 … ncol1, i=1, 2, 3…..8, l=1, 2, 3……10 ; d and λ are the antenna spacing and the signal wavelength respectively, and the *symbol is indicative of multiplication.

At the receiver side, there is a 4×8 sized rectangular planner antenna array with nrow2 (=4) × ncol2(=8) elements. The normalized receive array response vector corresponding to the lth ray in the ith cluster is given by

$$a_r(\phi_{il},\theta_{il})=\frac{1}{\sqrt{nrow2*ncol2}}[1,\ldots,e^{j\frac{2\pi}{\lambda}d(psin\varphi_{il}sin\theta_{il}+qcos\theta_{il})},\ldots e^{j\frac{2\pi}{\lambda}d\left((nrow-1)sin\varphi_{il}sin\theta_{il}+(ncol-1)cos\theta_{il}\right)}]^T \quad (3)$$

where, p=0, 1, 2……. Nrow2, q=0, 1, 2…... Ncol2, i=1, 2, 3….8, l=1, 2, 3……10; d and λ are the antenna spacing and the signal wavelength respectively [4, 10, 11]. The size of the normalized transmit array response vector $a_t(\phi_{il}^t,\theta_{il}^t)$ presented in Equation (2) is 8×32×80. Considering all the antenna array elements in 2-dimensional form to 1-dimensional form, the modified normalized transmit array response vector, $\hat{a}_t(\phi_{il}^t,\theta_{il}^t)$ will have a dimension of 256×80. Similarly, the size of the normalized receive array response vector $a_r(\phi_{il}^r,\theta_{il}^r)$ presented in Equation (3) is 8×4×80. Considering all the antenna array elements in 2-dimensional form to 1-dimensional form, the modified normalized receive array response vector, $\hat{a}_r(\phi_{il}^r,\theta_{il}^r)$ will have a dimension of 32×80.

2.4. Hybrid Precoding

In our presently considered simulated single-user mmWave massive MIMO NC- OFDM system, a transmitter with $N_t(=256)$ antennas communicate $N_s(=4)$ data streams to a receiver with $N_r(=32)$ antennas. The transmitter is equipped with $N_{tRF}(=4)$ transmitchains. The mmWave massive MIMO channel presented in Equation (1) has a size of 32 x 256 and it is further rescaled through multiplication with the normalization constant to get $E\|H\|_F^2=N_tN_r$.

To design the hybrid mmWave precoders (FRF; FBB), the rescaled mmWave channel matrix $\overline{H}$ undergoes singular value decomposition. As a result, we obtain $\overline{H}=U\sum V^T$ where $(\cdot)^T$ is indicative of complex conjugate transformation, U is a $N_r \times \text{rank}(\overline{H})$ unitary matrix and $V(=[V_1V_2])$ is a $N_t \times \text{rank}(\overline{H})$ unitary matrix. The matrix $\Sigma=\begin{bmatrix}\Sigma_1 & 0\\ 0 & \Sigma_2\end{bmatrix}$ is a $\text{rank}(\overline{H}) \times \text{rank}(\overline{H})$ diagonal matrix whose diagonal entries consist of singular values arranged in descending order. The $N_t \times N_s$ sized optimal unconstrained unitary precoder for $\overline{H}$ is simply given by $F_{opt}=V_1$. By defining the $N_t \times (N_{cl} \times N_{ray})$ sized normalized transmit array response vector presented in Equation (2) as A_t, the best RF beam forming vector can be selected from A_t and F_{opt}.

The optimal unconstrained hybrid mmWave precoders $(FRF_{unc}; FBB_{unc})$ can be estimated with the implementation of spatially sparse precoding via orthogonal matching pursuit. The optimal unconstrained hybrid mmWave precoders $(FRF_{unc}; FBB_{unc})$ are processed to estimate the constrained analog RF precoder FRF and the constrained baseband precoder FBB based on the assumption:

$$FRF_{unc}FBB_{unc}=F_{opt} \quad (4)$$

From equation (4), we can write,

$$FBB_{unc}=(FRF_{unc}^TFRF_{unc})^{-1}FRF_{unc}^TF_{opt} \quad (5)$$

where FRF_{unc}^T is the conjugate transformed form of FRF_{unc}.

Equation (5) can be written in a modified form as:

$$FRF_{unc}^TFRF_{unc}FBB_{unc}=FRF_{unc}^TF_{opt} \quad (6)$$

In Equation (6), the unknown FBB_{unc} can be determined iteratively with minimization of residual $r_1^{(i)}=FRF_{unc}^TF_{opt}-FRF_{unc}^TFRF_{unc}FBB_{unc}$ $^{(i)}$ using the Conjugate Gradient square method. The iteration terminates when the estimated residual value is $\leq 1\times10^{-10}$. The iteratively re-estimated value FBB_{unc} is FBB. Using the following relation

$$F_{opt}=FRFFBB \quad (7)$$

Equation (7) can be written in a modified form as:

$$FBB^TFRF=F_{opt}^T \quad (8)$$

where FBB^T and F_{opt}^T are the conjugate transformed form of FBB and F_{opt} respectively. In Equation (8), the unknown FRF can be determined iteratively with minimization of residual $r_1^{(i)}=F_{opt}^T-FBB^TFRF^{(i)}$ using the Conjugate Gradient square method.

To estimate the $N_r \times N_s$ sized optimal unconstrained combiner W_{opt}, the first N_s columns of $N_r \times N_r$ sized unitary matrix U are considered. The W_{opt} can be defined in terms of the unconstrained RF combiner WRF_{unc} and the uncontained baseband combiner WBB_{unc} as:

$$WRF_{unc}WBB_{unc}=W_{opt} \quad (9)$$

From equation (9), we can write

$$WBB_{unc}=(WRF_{unc}^TWRF_{unc})^{-1}WRF_{unc}^TW_{opt} \quad (10)$$

where, WRF_{unc}^T is the conjugate transformed form of WRF_{unc}. Equation (10) can be written in a modified form as:

$$WRF_{unc}^TWRF_{unc}WBB_{unc}=WRF_{unc}^TW_{opt} \quad (11)$$

In Equation (11), the unknown WBB_{unc} can be determined iteratively with minimization of residual $r_2^{(i)}=WRF_{unc}^TW_{opt}-WRF_{unc}^TWRF_{unc}WBB_{unc}$ $^{(i)}$ using the Conjugate Gradient square method. The iteration terminates when the estimated residual value is $\leq 1\times10^{-10}$. The iteratively re-estimated WBB_{unc} value is WBB. Using the following relation

$$W_{opt}=WRFWBB \quad (12)$$

Equation (12) can be written in modified form as:

$$\mathrm{WBB^{T}WRF} = \mathrm{W_{opt}^{T}} \tag{13}$$

where,$\mathrm{WBB^{T}}$and $\mathrm{W_{opt}^{T}}$are the conjugate transformed form of WBB and $\mathrm{W_{opt}}$, respectively. In Equation (15), the unknown WRF can be determined iteratively with minimization of residual $r_2^{(i)} = W_{opt}^{T} - WBB^{T}WRF^{(i)}$ using the Conjugate Gradient square method [12-14].

2.5. Group Detection (GD) Approach Aided Efficient Zero-Forcing (ZF)

Group detection (GD) approach based Efficient Zero-forcing (ZF) detectors can reduce the computational cost of conventional linear detectors. In our $\mathrm{N_r} \times \mathrm{N_t}$ MassiveMIMO system, the signal model can be represented by

$$\mathrm{y} = \mathrm{Hx} + \mathrm{n} \tag{14}$$

where, H is a channel matrix presented in Equation (1) with its (j, i)th entry$\mathrm{h_{ij}}$for the complex channel gain between the ith transmit antenna and the jth receive antenna, j=1, 2,. . . . . $\mathrm{N_r}$ and $\mathrm{i} = 1, 2, \ldots\ldots \mathrm{N_t}$, $\mathrm{x} = [\mathrm{x_1}, \mathrm{x_2}, \ldots\ldots\ldots \mathrm{x_{N_t}}]^{\mathrm{T}}$, and $\mathrm{y} = [\mathrm{y_1}, \mathrm{y_2}, \ldots\ldots\ldots \mathrm{y_{N_r}}]^{\mathrm{T}}$ are the transmitted and received signals and$\mathrm{n} = [\mathrm{n_1}, \mathrm{n_2}, \ldots\ldots\ldots, \mathrm{n_{N_R}}]^{\mathrm{T}}$ is the white Gaussian noise with a varianceσ_n^2. Equation (14) can be rewritten as:

$$\mathrm{y} = \begin{bmatrix}\overline{\mathrm{H}}_1 & \overline{\mathrm{H}}_2\end{bmatrix}\begin{bmatrix}\mathrm{s}_1 \\ s_2\end{bmatrix} + \mathrm{n} = \overline{\mathrm{H}}_1\mathrm{s}_1 + \overline{\mathrm{H}}_2\mathrm{s}_2 + \mathrm{n} \tag{15}$$

where,$\overline{\mathrm{H}}_1 \in \mathrm{C}^{\mathrm{N_r}\times\mathrm{L}}$ and $\overline{\mathrm{H}}_2 \in \mathrm{C}^{\mathrm{N_r}\times(\mathrm{N}-\mathrm{L})}$are composed of the first L and the remaining (N-L) columns of H, respectively. N is the total number of columns of H. Similarly, $\mathrm{s}_1 \in \mathrm{C}^{\mathrm{L}\times\mathrm{l}}$ and $\mathrm{s}_2 \in \mathrm{C}^{(N-L)\times l}$are the two sub symbol vectors that are created by taking the first L rows and the remaining rowsof x. Let us consider a weight matrix, $\mathrm{W}_1 = (\overline{\mathrm{H}}_1^{\mathrm{H}}\overline{\mathrm{H}}_1)^{-1}\overline{\mathrm{H}}_1^{\ \mathrm{H}}$, where $(\bullet)^{\mathrm{H}}$denotes a Hermitian transpose operation. If we multiply both sides of Equation (15) by W_1, we get

$$\mathrm{W}_1\mathrm{y} = \mathrm{s}_1 + \mathrm{W}_1\overline{\mathrm{H}}_2\mathrm{s}_2 + \mathrm{W}_1\mathrm{n} \tag{16}$$

Or equivalently, we can write

$$\mathrm{s}_1 = \mathrm{W}_1\mathrm{y} - \mathrm{W}_1\overline{\mathrm{H}}_2\mathrm{s}_2 - \mathrm{W}_1\mathrm{n} \tag{17}$$

Substituting equation (17) into equation (15) and after some mathematical manipulation, we get

$$\mathrm{y}_2 = \tilde{\mathrm{H}}_2\mathrm{s}_2 + \mathrm{n}_2 \tag{18}$$

where, $\mathrm{y}_2 \in \mathrm{C}^{\mathrm{N_R}\times 1}$, $\tilde{\mathrm{H}}_2 \in \mathrm{C}^{\mathrm{N_R}\times(\mathrm{N}-\mathrm{L})}$, and $\mathrm{n}_2 \in \mathrm{C}^{\mathrm{N_r}\times\mathrm{l}}$. The variables$\mathrm{y}_2$, $\tilde{\mathrm{H}}_2$, and$\mathrm{n}_2$can be rewritten as:

$$\mathrm{y}_2 = (\mathrm{I} - \overline{\mathrm{H}}_1\mathrm{W}_1)\mathrm{y} \tag{19}$$

$$\tilde{\mathrm{H}}_2 = (\mathrm{I} - \overline{\mathrm{H}}_1\mathrm{W}_1)\overline{\mathrm{H}}_2 \tag{20}$$

$$\mathrm{n}_2 = (\mathrm{I} - \overline{\mathrm{H}}_1\mathrm{W}_1)\mathrm{n} \tag{21}$$

where, I is an identity matrix. Based on the estimated $\tilde{\mathrm{H}}_2$and variables, we can define another weight matrix,W_2 as

$$W_2 = (\tilde{H}_2^H\tilde{H}_2)^{-1}\tilde{H}_2^H \tag{22}$$

The sub symbol vector$\mathrm{s}_2$is estimated using$\hat{\mathrm{s}}_2 = \mathrm{Q}(\mathrm{W}_1\mathrm{y}_1)$, where the symbol Q is indicative of quantization. The effect of$\mathrm{s}_2$is cancelled out from y to get$\mathrm{y}_1 = \mathrm{y} - \overline{\mathrm{H}}_2\hat{\mathrm{s}}_2$. The sub symbol vector s_1 is estimated using $\hat{\mathrm{s}}_1 = \mathrm{Q}(\mathrm{W}_1\mathrm{y}_1)$. The transmitted signal vector x is estimated as [15]:

$$\hat{x} = [\hat{s_1}^T\hat{s_2}^T]^T \tag{23}$$

2.6. Cholesky Decomposition (CD) based ZF Detection

In Cholesky Decomposition (CD) based ZF signal detection scheme, the signal model presented in Equation (14) is used and the matched filtering (MF) based detected signal is given by

$$\hat{\mathrm{x}}_{\mathrm{MF}} = \mathrm{H}^{\mathrm{H}}\mathrm{y} = \mathrm{H}^{\mathrm{H}}\mathrm{Hx} + \mathrm{H}^{\mathrm{H}}\mathrm{n} \tag{24}$$

where,$\mathrm{H}^{\mathrm{H}}$is the Hermitian conjugate of the estimated channel. In interference limited scenarios, a more advanced ZF detector is required which operates on the MF data given by

$$\hat{\mathrm{x}}_{\mathrm{ZF}} = (\mathrm{H}^{\mathrm{H}}\mathrm{H})^{-1}\hat{\mathrm{x}}_{\mathrm{MF}} \tag{25}$$

In Cholesky Decomposition (CD) based ZF detection, Equation (25) can be rewritten as:

$$\hat{\mathrm{x}}_{\mathrm{ZF}} = (\mathrm{H}^{\mathrm{H}}\mathrm{H})^{-1}\hat{\mathrm{x}}_{\mathrm{MF}} = (\mathrm{LL}^{\mathrm{H}})^{-1}\hat{\mathrm{x}}_{\mathrm{MF}} \tag{26}$$

With a forward and backward substitution, the detected signal in CD based ZF detection would be [16]

$$\hat{\mathrm{x}}_{\mathrm{ZF}} = \mathrm{L}^{-\mathrm{H}}\mathrm{L}^{-1}\hat{\mathrm{x}}_{\mathrm{MF}}. \tag{27}$$

2.7. LDPC Channel Coding

In 1962, Gallager invented Low-density parity-check (LDPC) linear block codes with its parity-check matrix H which contained only a few 1's in comparison to 0's. In his pioneer work, a bilateral Tanner graph was used to graphically represent the LDP Ccodes. The nodes of the LDPC block code were grouped into one set of n bit nodes (or variable nodes) and the other set of m check nodes (or parity nodes). The LDPC decoding scheme operates alternatively on the bit nodes and check nodes to find the most likely code word *c* that satisfies the condition$\mathrm{cH}^{\mathrm{T}} = 0$. In iterative Log Domain Sum-Product LDPC decoding under scenario of AWGN noisy channel of varianceσ^2 and received signal vector r, log-likelihood ratios (LLRs) instead of probability are generally defined as:

$$\mathrm{L}(\mathrm{c_i}) \triangleq \ln[\mathrm{P}(\mathrm{c_i} = 0 \mid \mathrm{r_i})/\mathrm{P}(\mathrm{c_i} = 1 \mid \mathrm{r_i})] \tag{28}$$

$$\mathrm{L}(\mathrm{P_{ij}}) \triangleq \ln[\mathrm{P_{ij}^0}/\mathrm{P_{ij}^1}) \tag{29}$$

$$\mathrm{L}(\mathrm{Q_{ij}}) \triangleq \ln[\mathrm{Q_{ij}^0}/\mathrm{Q_{ij}^1}) \tag{30}$$

$$L(P_j) \triangleq \ln[P_j^0/P_j^1) \quad (31)$$

where$\ln(\cdot)$represents the natural logarithm operation. The bit node j is initially set with an edge to check node i:

$$L(P_{ij}) = L(c_i) = 2r_i/\sigma^2 \quad (32)$$

In message passing from check nodes to bit nodes for each check node *i* with an edge to bit node j; $L(Q_{ij})$ is updated as:

$$L(Q_{ij}) = \Pi_{j'}\alpha_{ij'}\phi[\Sigma_{j'}\phi(\beta_{ij'})]\ (j'1, 2, \ldots\ldots n \text{ and } j' \neq j) \quad (33)$$

where, $\alpha_{ij} \triangleq \text{sign}[L(P_{ij})]$ and $\beta_{ij} \triangleq [L(P_{ij})]$. The$\phi$function is defined as:

$$\phi x = -\ln[\tanh(x/2)] = \ln[(e^x + 1)/(e^x - 1)] \quad (34)$$

From bit nodes to check nodes for each bit node j with an edge to check node i; $L(P_j)$is updated as:

$$L(P_{ij}) = L(c_i) + \Sigma_{i'}L(Q_{ij})] \quad (35)$$

where $(i' = 1, 2, \ldots\ldots \text{mand} i' \neq i)$. With decoding and soft outputs for j=1, 2,...., n; $L(P_j)$ is updated as:

$$L(P_j) = L(c_i) + \Sigma_i L(P_{ij})](i = 1, 2\ldots\ldots m) \quad (36)$$

$$c_i = \begin{cases} 1 \text{ if} L(P_j) < 0 \\ 0 \text{ else} \end{cases} \quad (37)$$

If $cH^T = 0$ or the number of iterations reaches the maximum limit [17].

2.8. (3, 2) SPC Channel Coding

Transmitted binary bits are rearranged into very small code words consisting of merely two consecutive bits in SPC channel coding. In such channel coding, (3, 2) SPC code is used with addition of a single parity bit to the message u = [u0, u1] so that the elements of the resulting code word x = [x0, x1, x2] are given by x0 = u0, x1 = u1 and x2 = u0Θu1. Here Θis considered to denote the sum over GF (2) [18].

2.9. 2D Median Filtering

2D median filtering is widely used as an effective and reliable technique for removing various types of noises. In this filtering operation, the pixel values of an image in the neighborhood window are generally ranked according to intensity and the middle value (the median) becomes the output value for the pixel under evaluation. The applicability of 2D Median Filtering scheme has been made in our work by using a 3×3 neighborhood windowing mask which sorts out all the pixel values within the window and estimates the median value. This median value replaces the original pixel value [19].

3. System Description

The conceptual block diagram of the 5G compatible WO scheme implemented hybrid precoded mmWave massive MIMO NC- OFDM system is shown in Figure 1. In this system, an RGB color image is processed and is primarily converted into its respective three red, green, and blue components. The pixel integer to binary converted digital signal is channel coded and interleaved and digitally modulated using preferable higher order digital modulations [20]. The digitally modulated complex symbols undergoes serial–to–parallel conversion and are fed into the NC-OFDM subcarrier selection section and subsequently processed for multicarrier modulation, parallel to serial conversion, cyclic prefixing and cyclic post fixing insertion, Tukey (tapered cosine) windowing and fed into spatial multiplexing encoder [8].

The encoded signals in four data streams are precoded with a digital baseband precoder, D/A conversion and subsequently sent up into analog RF precoder prior to transmission. In the receiving section, the signals are processed with an analog RF combiner, A/D converter, digital baseband combiner, and a spatial multiplexing decoder to produce signal in a single data stream. From the single streamed processed signal, cyclic prefixing and post fixing are removed and it is converted in a serial–to–parallel manner, multicarrier demodulated and the NC-OFDM subcarrier symbols are extracted. The extracted complex digitally modulated symbols are parallel to serial converted, digitally demodulated, deinterleaved, channel decoded, binary to integer converted, filtered, and the R, G, B components are extracted and eventually the retrieved color image is obtained.

4. Results and Discussion

In this subsection, the system performance in terms of simulated BER results using MATLAB R2017a have been presented to illustrate the significant impact of various types of channel coding and signal detection techniques on the performance analysis of a 5G Compatible WO scheme implemented Hybrid Precoded mmWave massive MIMO non-contiguous OFDM system. The present study is based on the assumption that the Channel state information (CSI) of the mmWave Massive MIMO Rayleigh fading channel is available at the receiver and the fading channel coefficients are constant during simulation. The proposed model is simulated to evaluate the system performance under consideration of the parameters presented in Table 1.

Table 1. *Summary of the simulated model parameters.*

Parameters	Types
Data type	Color Image
Image Size	(3 ×192 × 256) pixels
Noise reduction image filter	2D-Median filter

Parameters	Types
No of subcarriers	1024
CP Length	128 samples
Carrier frequency	38 GHz
Window length, WLat both ends of Tukey (tapered cosine) windowing function	40, 60 and 80 samples
Pulse shaping filter	Raised cosine filter with roll off 0.25 and filter order 40
Antenna configuration	32× 256 massive MIMO Channel
Channel Coding	(3, 2) SPC) and LDPC
LDPC Channel decoding	Log-domain sum product
Constellation Modulation	64-QAM, 128-QAM and 256-QAM, 64-PSK, 128-PSK and 256-PSK
Signal Detection Scheme	GroupDetection (GD) approach aided Efficient Zero-Forcing (ZF)and Cholesky Decomposition(CD) based ZF detection
SNR	0 to 15 dB
Channel	AWGN and Rayleigh

The graphical illustration presented in Figure 2 elaborates the performance of the simulated system in terms of bit error rate (BER) vs. signal to noise ratio (SNR) values. With implementation of 256-QAM, (3, 2) SPC channel coding, Zero-Forcing based Group detection technique under consideration of different Tukey windowing length, it is observable that the system performance deteriorates with increase in Tukey windowing length. For a typically assumed SNR value of 2 dB, the estimated BERs are found to have values of 0.151, 0.1533 and 0.1609 in case of Tukey windowing length of 40, 60 and 80 respectively. It is important to note that for this specifically considered SNR value, the system performance improvement of 0.0656 dB and 0.2757 dB are achieved in Tukey windowing length of 40 as compared to Tukey windowing length of 60 and 80. At 10^{-1}BER, SNR gains of 5.5, 6 and 7 are obtained in Tukey windowing length of 40, 60 and 80.

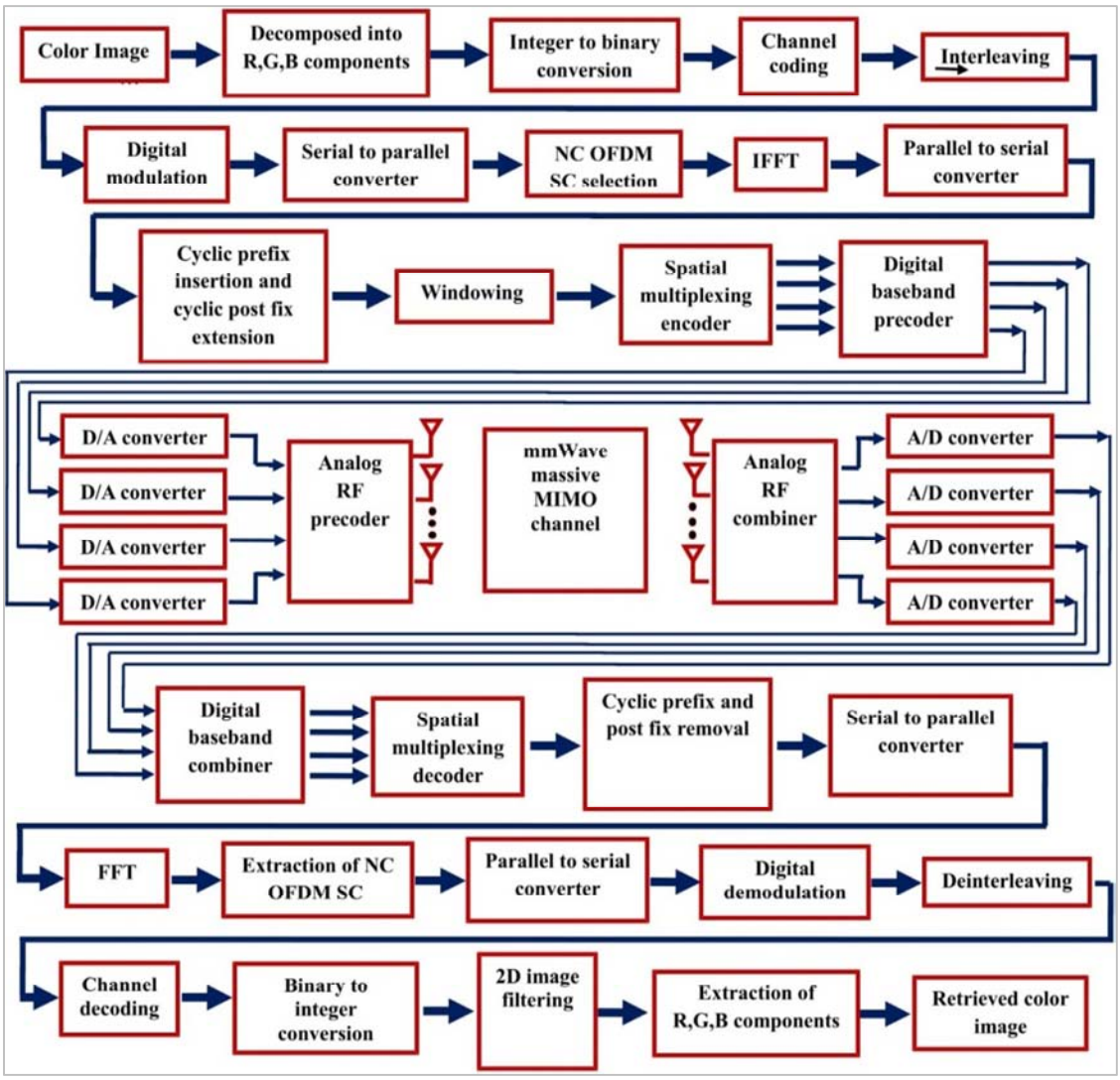

Figure 1. *Block diagram of a 5G Compatible WO scheme implemented Hybrid Precoded mmWave massive MIMO NC- OFDM system.*

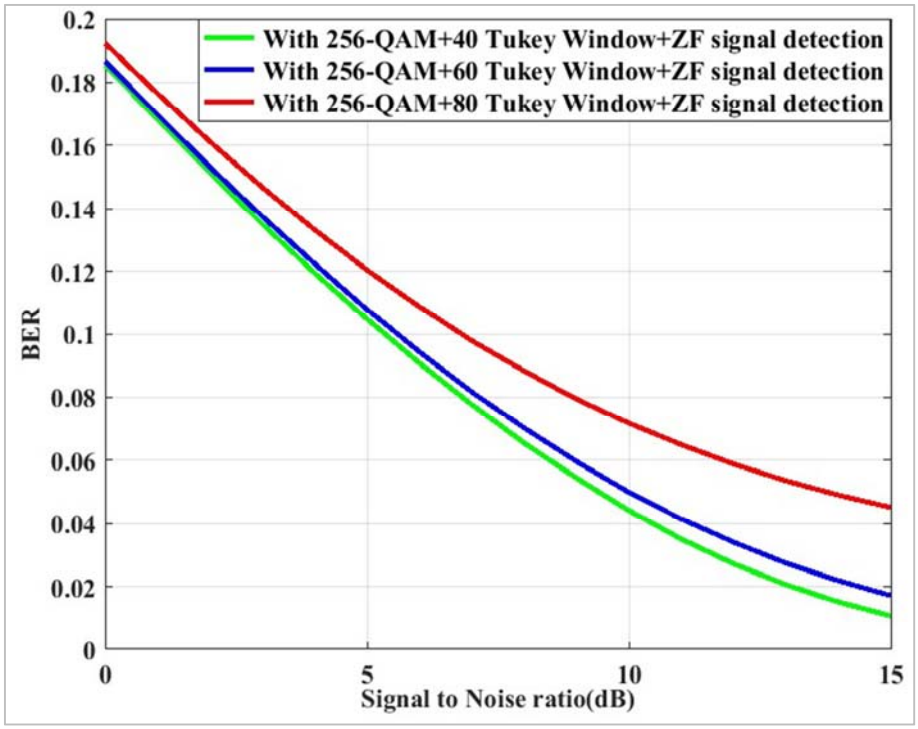

Figure 2. *Effect of identical length (samples) of cosine-tapering part at both ends of Tukey (tapered cosine) window on BER performance of the simulated system under utilization of 256-QAM, (3, 2) SPC channel coding and Zero-Forcing based Group detection schemes.*

Figure 3 depicts the numerically evaluated BER performance of the simulated system with implementation of Tukey windows of various lengths, Cholesky decomposition-based signal detection and higher order digital modulation (256 QAM). It is observed that the simulated system outperforms when we use a Tukey window of comparatively lesser length. The required SNR at the BER 10^{-1} is found to have value of 6.5 dB at Tukey windowing length of 80. It is reduced to 6 dB and 5.5 dB with window lengths of 60 and 40 respectively.

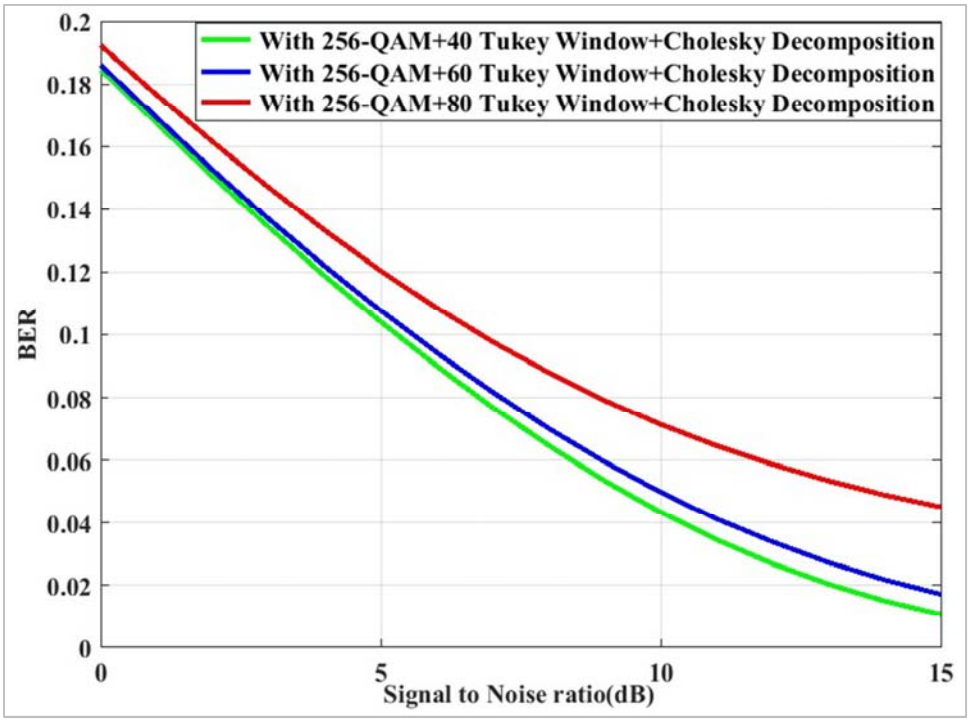

Figure 3. *Effect of identical length (samples) of cosine-tapering part at both ends of Tukey (tapered cosine) window on BER performance of the simulated system under utilization of 256-QAM, (3, 2) SPC channel coding and Cholesky Decomposition based signal detection schemes.*

In Figure 4, the BERs for the simulated system in terms of different values of SNR are plotted using the LDPC channel coding and Zero-Forcing based Group detection schemes. We can see that when the BER is 10^{-1}, the SNRs required for Tukey windowing lengths of 40, 60 and 80 are 11.5 dB, 11.9 dB and 12.5 dB respectively. For a typical assumed SNR value of 2 dB, the estimated BER values are 0.2529, 0.2540 and 0.2598 which ratify the system performance improvement of 0.0188 dB and 0.0980 dB in Tukey windowing length of 40 as compared to Tukey windowing length of 60 and 80.

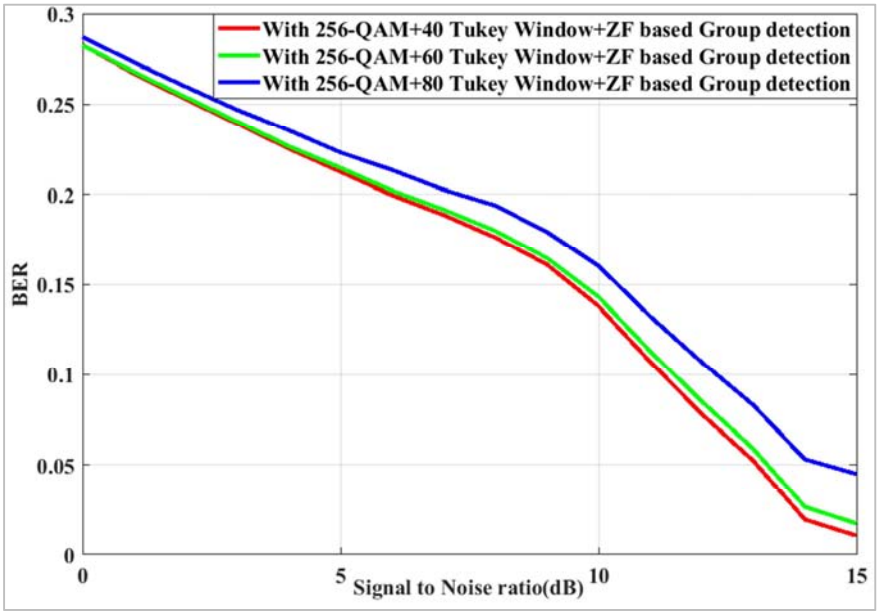

Figure 4. *Effect of identical length (samples) of cosine-tapering part at both ends of Tukey (tapered cosine) window on BER performance of the simulated system under utilization of 256-QAM, LDPC channel coding and Zero-Forcing based Group detection schemes.*

Figure 5 shows the impact of implementing the LDPC channel coding and Cholesky decomposition based signal detection scheme on system performance. Based on presented curves in Figure 5, it is quite evident that at a SNR value of 2dB, the estimated BERs are 0.2524, 0.2538 and 0.2599 which provide indication of system performance improvement of 0.0240 dB and 0.1031 dB in Tukey windowing length of 40 in comparison with Tukey windowing length of 60 and 80.

In Figure 6, it is noticeable that the curves are well-defined. The required SNR at the BER $10^{-1}$is 5.5 dB for 256 QAM digital modulation. It is reduced to 3 dB and 0.5 dB with the descending order of digital modulation (128 QAM and 64 QAM). For a typical assumed SNR value of 2 dB, the estimated BER values are 0.0785, 0.1189 and 0.1519 which are indicative of system performance improvement of 1.803 dB and 2.867 dB in 64 QAM as compared to 128QAM and 256QAM.

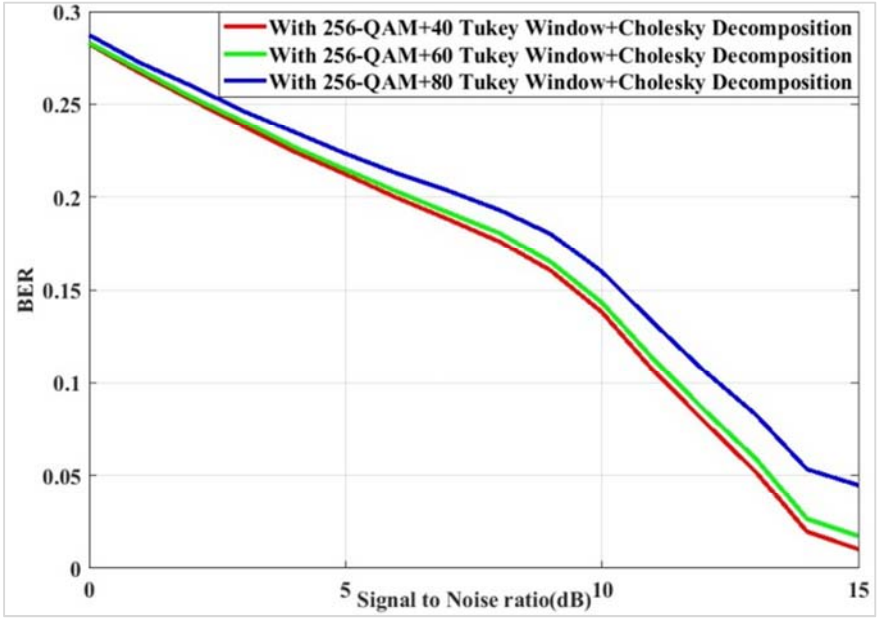

Figure 5. *Effect of identical length (samples) of cosine-tapering part at both ends of Tukey (tapered cosine) window on BER performance of the simulated system under utilization of 256-QAM, LDPC channel coding and Cholesky Decomposition based signal detection schemes.*

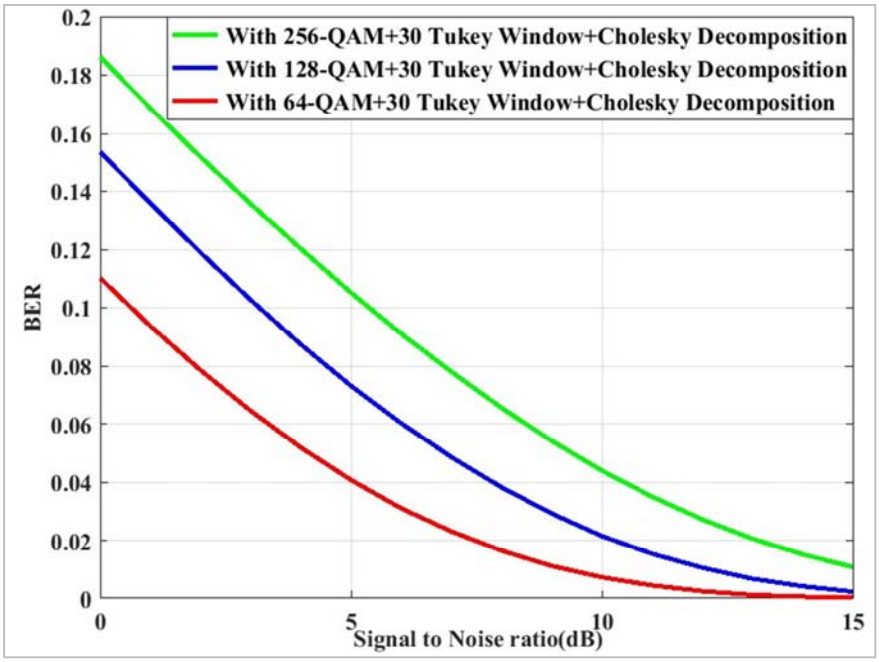

Figure 6. *Effect of QAM modulation of different orders on BER performance of the simulated system under utilization of Tukey windowing of sample length 30, (3, 2) SPC channel coding and Cholesky Decomposition based signal detection schemes.*

The graphical illustration presented in Figure 7 clearly indicates that utilization of PSK based different digital modulations causes the simulated system to show poor performance as compared to the results presented in the previous figures. At 20% BER, the SNR with the higher order PSK modulation (256-PSK) is 12 dB. It is reduced to 7.5 dB and 4 dB in case of 128-PSK and 64-PSK digital modulations respectively. The presented curves also confirm that the system performance deteriorates with an ascending order of digital modulation.

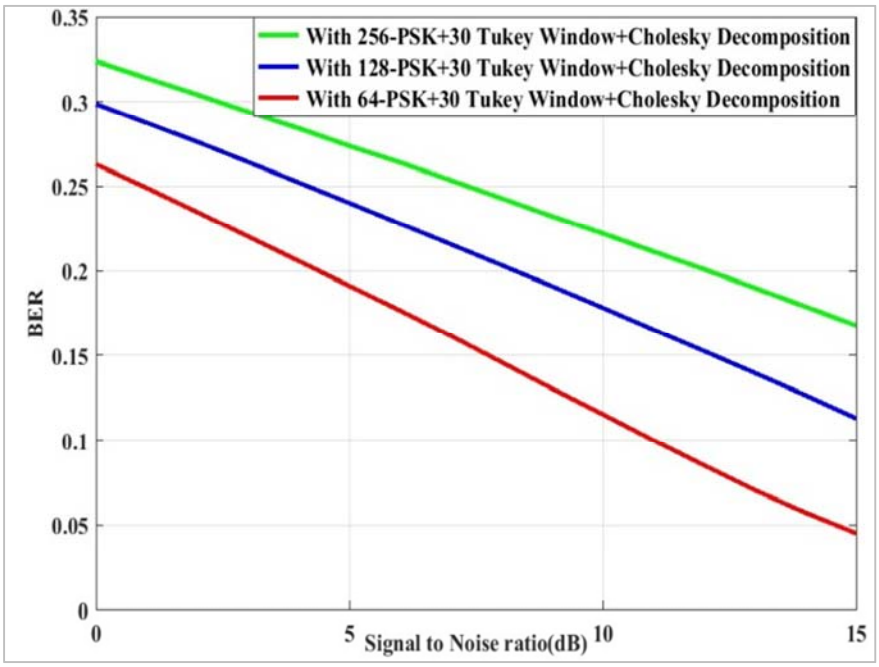

Figure 7. *Effect of PSK modulation of different orders on BER performance of the simulated system under utilization of Tukey windowing of sample length 30, (3, 2) SPC channel coding and Cholesky Decomposition based signal detection schemes.*

Figure 8 shows the transmitted and retrieved color images without filtering and with filtering for a 10 dB SNR value for higher order (256-QAM) digital modulation under implementation of the Cholesky decomposition-based signal detection (3, 2) SPC channel coding and 40 Tukey windowing samples. Figure 8 also ratifies that the quality of the retrieved images is improved with the application of a 2D image noise reduction technique.

The histograms presented in Figure 9 clearly show the distribution of pixel values of RGB to Gray converted retrieved color images. Based on Figure 9, it is apparent that the additional pixel values in the upper range are found to occur in the filtered gray converted image.

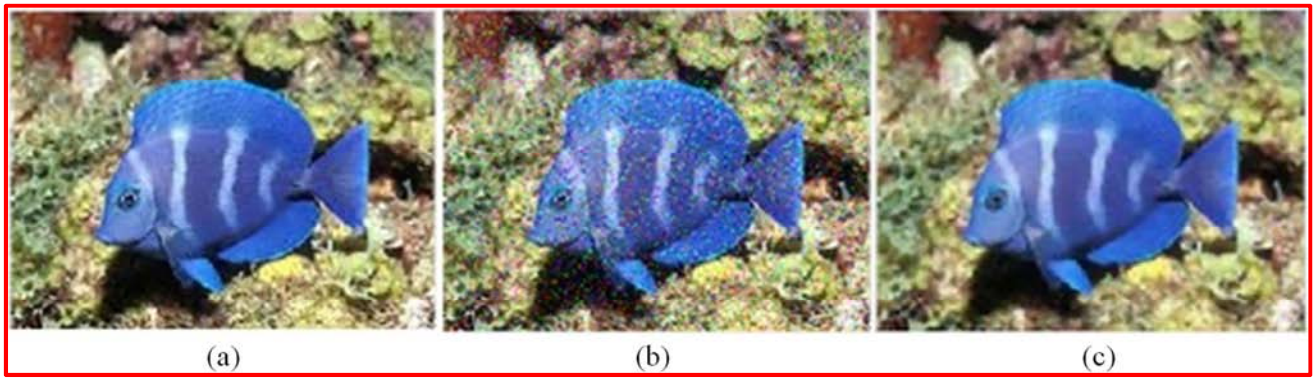

Figure 8. *Transmitted and retrieved color images with and without filtering at 10 dB SNR value with utilization of 256-QAM digital modulation, Cholesky decomposition-based signal detection,(3, 2) SPC channel coding and 40 Tukey windowing samples, (a) Original image(b) Image without filtering and (c)Filtered image.*

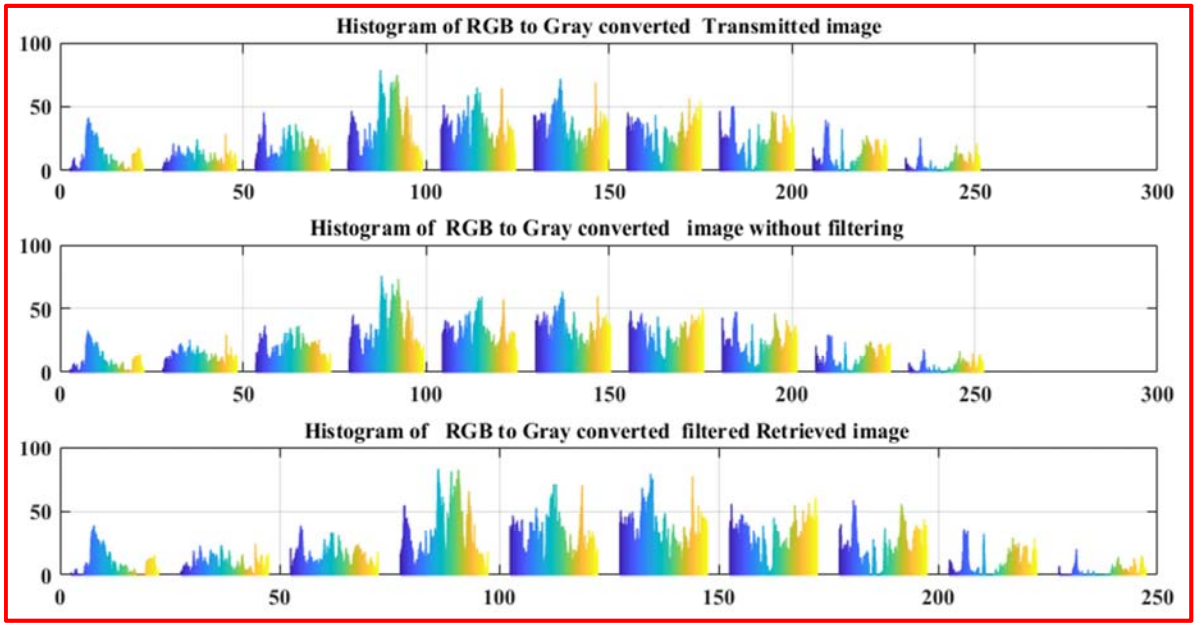

Figure 9. *Histograms of RGB to Gray converted Retrieved color images with and without filtering at 10 dB SNR value under utilization of 256-QAM digital modulation, Cholesky decomposition-based signal detection,(3, 2) SPC channel coding and 40 Tukey windowing samples.*

5. Conclusion

In this paper, the performance of a 5G Compatible WO scheme implemented Hybrid Precoded mmWave massive MIMO NC- OFDM system has been investigated on color image transmission with the utilization of various channel coding and channel equalization/signal detection techniques.

The simulation results show that the implementation of Cholesky decomposition-based signal detection and (3, 2) SPC channel coding techniques enhances the system performance. Based on our results, we have also shown that with reduction of the window length of Tukey (tapered cosine) windowing function results in improvement of the performance of simulated system. Application of image filtering techniques ratifies that the quality of the retrieved image is improved and more visible.

References

[1] Adrian Kliks, Hanna Bogucka, and Paweł Kryszkiewicz. Multicarrier Technologies for Future Radio Communication 5G and Beyond. John Wiley and Sons, Inc, USA, 2017.

[2] Shaik Yasmin Fathima, Muhammad Zia Ur Rahman, K. Murali Krishna, Shakira Bhanu, and Mirza Shafi Shahsavar,"Side Lobe Suppression in NC-OFDM Systems Using Variable Cancellation Basis Function", IEEE Access, vol.5, pp. 9415 - 9421 , 2017.

[3] Atif Elahi, Mehreen Atif, Ijaz Mansoor Qureshi, and Noor Gul,"Interference Reduction in Cognitive Radio Networks Using Genetic and Firefly Algorithms", In Proceeding of International Conference on Communication, Computing and Digital Systems (C-CODE), pp. 96 – 100, 2017.

[4] Shahid Mumtaz, Jonathan Rodriguez, and Linglong Dai. mmWave Massive MIMO A Paradigm for 5G. In mmWave Massive MIMO A Paradigm for 5G. Elsevier Inc Academic Press, an imprint of Elsevier Inc, 2017.

[5] De-Zhuang Qin ; Jin-An Ren ; Yi-Hu Xu,"An Efficient Pruning Algorithm for IFFT/FFT Based on NC-OFDM in 5G", In proceeding of Second International Conference on Inventive Communication and Computational Technologies (ICICCT), pp.432 – 435, 2018.

[6] Lilin Dan; Chiheng Zhang ; Jie Yuan ; Peibo Wen ; Bin Fu, "Improved N-continuous OFDM using adaptive power allocation", In proceeding of IEEE 8th Annual Computing and Communication Workshop and Conference (CCWC), pp. 937 – 940, 2018.

[7] Changyoung An, Jungu Lee, and Heung-Gyoon Ryu,"An spectrum Efficient WO-OFDM using Windowing and Overlapping on the Cyclic Prefix and Postfix", In proceedings of the IEEE International Conference on Recent Advances in Signal Processing, Telecommunication and Computing (SigTelCom), pp.198 – 202, 2018.

[8] Tangina Sultana, M. S. Ara Showkat, Mohammad Shah Alam, Md. Delowar Hossain, and Ashis Kumar Mandal "Reducing Peak to Average Power Ratio of OFDM Signals using Tukey Window Technique". International Journal of Scientific Engineering and Technology, vol. 2, issue 9, pp.879–883, 2013.

[9] Shu Sun, Theodore S. Rappaport, Sundeep Rangan, Timothy A. Thomas, Amitava Ghosh, Istvan Z. Kovocs, Ignacio Rodriguez, Ozge Koymen, Andrzej Partyka, and Jan Jarvelainen,"Propagation Path Loss Models for 5G Urban Microand Macro-Cellular Scenarios", In Proceeding of IEEE 83rd Vehicular Technology Conference (VTC Spring), pp. 1-6, 2016.

[10] Xianghao Yu, Juei-Chin Shen, Jun Zhang, and Khaled B. Letaief "Alternating Minimization Algorithms for Hybrid Precoding in Millimeter Wave MIMO Systems", IEEE Journal of Selected Topics in Signal Processing, vol.10, issue 3, pp. 485–500, 2016.

[11] Stefano Buzzi and Carmen D' Andrea, "On clustered statistical MIMO millimeter wave channel simulation", ARXIV, available at https://arxiv.org/abs/1604. 00648, May 2016.

[12] Omar El Ayach, Sridhar Rajagopal, Shadi Abu-Surra, Zhouyue Pi, and Robert W. Heath Jr.,"Spatially Sparse Precoding in Millimeter Wave MIMO Systems", IEEE Transactions on Wireless Communications, vol.13, issue 3, pp. 1499 - 1513, 2014.

[13] Richard Barrett, Michael Berry, Tony F. Chan, James Demmel, June M. Donato, Jack Dongarra, Victor Eijkhout, Roldan Pozo, Charles Romine, and Henk Van der Vorst. Templates for the Solution of Linear Systems: Building Blocks for Iterative Methods. In Templates for the Solution of Linear Systems: Building Blocks for Iterative Methods, Philadelphia, SIAM publisher, USA, 1994.

[14] Weiheng Ni, Xiaodai Dong, and Wu-Sheng Lu, "Near Optimal Hybrid Processing for Massive MIMO Systems via Matrix Decomposition", In Proceeding of IEEE Transactions on Signal Processing, vol.65, issue 15, pp. 3922 – 3933, 2017.

[15] Thanh-Binh Nguyen, Tien-Dong Nguyen, Minh-Tuan Le, and Vu-Duc Ngo,"Efficiency Zero-Forcing Detectors based on Group Detection for Massive MIMO systems", In proceeding of International Conference on Advanced Technologies for Communications (ATC), pp.48 – 53, 2017.

[16] Rakesh Gangarajaiah, Hemanth Prabhu, Ove Edfors, and Liang Liu,"A Cholesky Decomposition based Massive MIMO Uplink Detector with Adaptive Interpolation", In proceeding of IEEE International Symposium on Circuits and Systems (ISCAS), pp.1-4, 2017.

[17] Yuan Jiang, A Practical Guide to Error-Control Coding Using MATLAB, Artech House Norwood, MA, USA, 2010.

[18] Giorgio M. Vitetta, Desmond P. Taylor, Giulio Colavolpe, Fabrizio Pancaldi, and Philippa A. Martin, Wireless Communications Algorithmic Techniques, John Wiley and Sons Ltd. United Kingdom, 2013.

[19] Oge Marques, Practical Image and Video Processing Using MATLAB, John Wiley and Sons, New Jersey, USA, 2011.

[20] Theodore S. Rappaport, Wireless Communications Principles and Practice, Prentice Hall, New Jersey, USA, 1996.